

A 4 Time-Dependent Density-Functional Theory

Arno Schindlmayr

Institut für Festkörperforschung

Forschungszentrum Jülich GmbH

Contents

1	Introduction	2
2	Theoretical Foundations	2
2.1	The Runge-Gross Theorem	3
2.2	The Time-Dependent Kohn-Sham Equations	5
2.3	Excited States	7
2.4	Linear-Response Theory	8
2.5	The Exchange-Correlation Kernel	9
3	Applications in Theoretical Spectroscopy	12
3.1	Electron Energy-Loss Spectroscopy	12
3.2	Optical Absorption	14
4	Summary	17

1 Introduction

Time-dependent density-functional theory (TDDFT) extends the basic ideas of static density-functional theory to the more general situation of systems subject to the influence of time-dependent external fields. It relies on the electron density $n(\mathbf{r}, t)$ instead of the many-body wave function $\Psi(\mathbf{r}_1, \dots, \mathbf{r}_N; t)$ and constitutes an efficient method to determine the dynamics of a quantum-mechanical system. The advantage over a direct solution of the time-dependent Schrödinger equation lies in the reduced computational complexity, because in addition to the time variable t the density depends only on a single coordinate vector \mathbf{r} , while the wave function depends on the positions $\mathbf{r}_1, \dots, \mathbf{r}_N$ of all electrons, where N may be a very large number. As in static density-functional theory, the standard way to obtain $n(\mathbf{r}, t)$ is with the help of an auxiliary system of noninteracting electrons. These so-called Kohn-Sham electrons move in a time-dependent local effective potential, whose exact functional form is unknown and must be approximated in practical implementations. The final equations can then easily be solved by numerical techniques even for systems with a large number of atoms.

The scheme is perfectly general and can be employed to describe essentially any time-dependent phenomenon, including nonlinear processes like the ionisation of atoms or molecules in strong laser fields. If the time-dependent potential is weak, on the other hand, linear-response theory is sufficient to study the dynamics of a system. In particular, this is often the case in condensed-matter physics, where irradiation with light or particle beams is the most important experimental technique to probe the electronic structure of a material. Electron energy-loss spectroscopy (EELS) and optical absorption are typical examples that can be treated within linear-response theory. The resulting spectra contain direct information about the excited states of the electron system. As the investigation of excited states constitutes the principal application of TDDFT in condensed-matter physics, it is also at the centre of this chapter. It should be noted that the method can only be used to study neutral excitations where the number of particles remains constant, such as charge oscillations (plasmons) in metals or bound electron-hole pairs (excitons) in semiconductors. The latter form if electrons are excited from the valence into the conduction band without sufficient kinetic energy to overcome the attractive Coulomb potential of the hole left behind. TDDFT is thus complementary to the GW approximation in many-body perturbation theory, which is related to photoemission spectroscopy and describes processes in which the particle number in the sample changes due to the ejection or injection of electrons.

This chapter is organised as follows. Section 2 introduces the theoretical framework of TDDFT. In line with the general focus on condensed-matter physics, special emphasis is placed on the linear-response regime and its connection to the electronic excitation spectrum. Section 3 then discusses selected applications to solids, namely the theoretical treatment of electron energy-loss spectroscopy and optical absorption. As the accuracy of the calculations is, above all, limited by the employed exchange-correlation functional, the performance of common approximations in reproducing the experimental spectra receives particular attention. Finally, Section 4 summarises the central points of this chapter.

2 Theoretical Foundations

As the quantum-mechanical treatment of stationary and time-dependent systems differs in many aspects, it is not straightforward to generalise the mathematical framework of static density-functional theory. For example, the total energy, which plays a central role in the original

Hohenberg-Kohn theorem [1], is not a conserved quantity in the presence of time-dependent external fields, and there is hence no variational principle for it on the basis of the density that can be exploited. For this reason, we must start anew and develop the theoretical foundations of TDDFT from scratch.

2.1 The Runge-Gross Theorem

The Runge-Gross theorem [2] is the equivalent of the Hohenberg-Kohn theorem for time-dependent systems and asserts the one-to-one correspondence between the external potential and the density, albeit with an important restriction. In contrast to the static Schrödinger equation, which is a second-order differential equation and constitutes a mathematical boundary-value problem whose possible eigenstates are determined by normalisation constraints, the time-dependent Schrödinger equation

$$i\hbar \frac{\partial}{\partial t} \Psi(\mathbf{r}_1, \dots, \mathbf{r}_N; t) = H(t) \Psi(\mathbf{r}_1, \dots, \mathbf{r}_N; t) \quad (1)$$

is of first order and a prototype example of an initial-value problem; its solution always requires the knowledge of the wave function $\Psi(\mathbf{r}_1, \dots, \mathbf{r}_N; t_0)$ at an initial time t_0 . The integration of Eq. (1) then describes the complete evolution of the system, but observables always depend on the initial state. For this reason, the Runge-Gross theorem only holds for a fixed initial state.

Of course, for a given external potential $V_{\text{ext}}(\mathbf{r}, t)$ it is always possible, in principle, to solve the time-dependent Schrödinger equation with the Hamiltonian

$$H(t) = \sum_{k=1}^N \left(-\frac{\hbar^2}{2m} \nabla_k^2 + V_{\text{ext}}(\mathbf{r}_k, t) \right) + \frac{1}{2} \sum_{k \neq l} v(\mathbf{r}_k - \mathbf{r}_l), \quad (2)$$

where $v(\mathbf{r} - \mathbf{r}') = e^2/|\mathbf{r} - \mathbf{r}'|$ denotes the Coulomb interaction. From the many-body wave function, the density is obtained according to

$$n(\mathbf{r}, t) = N \int |\Psi(\mathbf{r}, \mathbf{r}_2, \dots, \mathbf{r}_N; t)|^2 d^3r_2 \dots d^3r_N. \quad (3)$$

What we have to prove, in order to demonstrate the one-to-one correspondence, is that if two potentials $V_{\text{ext}}(\mathbf{r}, t)$ and $V'_{\text{ext}}(\mathbf{r}, t)$ differ by more than a purely time-dependent function, then the associated densities $n(\mathbf{r}, t)$ and $n'(\mathbf{r}, t)$ are always distinct. The addition of a purely time-dependent function is exempt because it only changes the phase of the wave function but not the density. In the following we assume that the two systems evolve from physically equivalent wave functions $\Psi(\mathbf{r}_1, \dots, \mathbf{r}_N; t_0)$ and $\Psi'(\mathbf{r}_1, \dots, \mathbf{r}_N; t_0)$, i.e., wave functions that differ at most by a constant phase factor at an initial time t_0 . Of course, this implies $n(\mathbf{r}, t_0) = n'(\mathbf{r}, t_0)$. Furthermore, we only admit potentials that vary smoothly in time and can be expanded into Taylor series

$$V_{\text{ext}}(\mathbf{r}, t) = \sum_{k=0}^{\infty} \frac{c_k(\mathbf{r})}{k!} (t - t_0)^k \quad \text{with} \quad c_k(\mathbf{r}) = \left. \frac{\partial^k}{\partial t^k} V_{\text{ext}}(\mathbf{r}, t) \right|_{t=t_0} \quad (4)$$

and analogously for $V'_{\text{ext}}(\mathbf{r}, t)$. If the two potentials differ by more than a purely time-dependent function, then at least one of the coefficients $u_k(\mathbf{r}) = c_k(\mathbf{r}) - c'_k(\mathbf{r})$ must not be a mere constant but a spatially varying function.

The proof of the Runge-Gross theorem employs the current density

$$\mathbf{j}(\mathbf{r}, t) = \frac{N}{2m} \int \Psi^*(\mathbf{r}, \mathbf{r}_2, \dots, \mathbf{r}_N; t) [-i\hbar \nabla \Psi(\mathbf{r}, \mathbf{r}_2, \dots, \mathbf{r}_N; t)] d^3r_2 \dots d^3r_N \quad (5)$$

$$- \frac{N}{2m} \int [-i\hbar \nabla \Psi^*(\mathbf{r}, \mathbf{r}_2, \dots, \mathbf{r}_N; t)] \Psi(\mathbf{r}, \mathbf{r}_2, \dots, \mathbf{r}_N; t) d^3r_2 \dots d^3r_N ,$$

which is related to the density through the continuity equation

$$\frac{\partial}{\partial t} n(\mathbf{r}, t) = -\nabla \cdot \mathbf{j}(\mathbf{r}, t) . \quad (6)$$

This identity expresses the conservation of the total particle number in a differential form: the change in the number of electrons within a certain volume equals the flux through its surface. In the first step, we show that the current densities $\mathbf{j}(\mathbf{r}, t)$ and $\mathbf{j}'(\mathbf{r}, t)$ induced by the two potentials differ. To this effect we examine the time derivative

$$\frac{\partial}{\partial t} [\mathbf{j}(\mathbf{r}, t) - \mathbf{j}'(\mathbf{r}, t)]_{t=t_0} = -\frac{1}{m} n(\mathbf{r}, t_0) \nabla [V_{\text{ext}}(\mathbf{r}, t_0) - V'_{\text{ext}}(\mathbf{r}, t_0)] = -\frac{1}{m} n(\mathbf{r}, t_0) \nabla u_0(\mathbf{r}) , \quad (7)$$

which follows from the definition (5) together with the known behaviour of the wave function (1) and its complex conjugate. If $u_0(\mathbf{r})$ is not a constant, then the right-hand side is nonzero, and consequently the derivatives of the current densities at t_0 must be different. Otherwise we take an appropriate higher time derivative

$$\frac{\partial^{k+1}}{\partial t^{k+1}} [\mathbf{j}(\mathbf{r}, t) - \mathbf{j}'(\mathbf{r}, t)]_{t=t_0} = -\frac{1}{m} n(\mathbf{r}, t_0) \nabla u_k(\mathbf{r}) \quad (8)$$

with a nonconstant $u_k(\mathbf{r})$ to establish that at least one term in the Taylor expansions of $\mathbf{j}(\mathbf{r}, t)$ and $\mathbf{j}'(\mathbf{r}, t)$ differs. This implies that the current densities themselves deviate for $t > t_0$.

In the second step we prove that the corresponding densities also differ. For this purpose we take the $(k+1)$ st time derivative of the continuity equation (6) and again examine the difference

$$\frac{\partial^{k+2}}{\partial t^{k+2}} [n(\mathbf{r}, t) - n'(\mathbf{r}, t)]_{t=t_0} = -\nabla \cdot \frac{\partial^{k+1}}{\partial t^{k+1}} [\mathbf{j}(\mathbf{r}, t) - \mathbf{j}'(\mathbf{r}, t)]_{t=t_0} = \frac{1}{m} \nabla \cdot [n(\mathbf{r}, t_0) \nabla u_k(\mathbf{r})] \quad (9)$$

between the two systems. The quantity on the right-hand side of this equation is nonzero. This implies that the $(k+2)$ nd terms in the Taylor expansions of $n(\mathbf{r}, t)$ and $n'(\mathbf{r}, t)$ around t_0 differ. As a consequence, the densities generated by the two distinct potentials $V_{\text{ext}}(\mathbf{r}, t)$ and $V'_{\text{ext}}(\mathbf{r}, t)$ themselves must deviate for $t > t_0$. This concludes the proof of the Runge-Gross theorem.

As we required the wave functions $\Psi(\mathbf{r}_1, \dots, \mathbf{r}_N; t_0)$ and $\Psi'(\mathbf{r}_1, \dots, \mathbf{r}_N; t_0)$ to be equivalent, the Runge-Gross theorem applies only to densities evolving from the same initial state. In fact, it is possible to construct systems with different initial states evolving in different time-dependent potentials whose densities nevertheless coincide exactly at all times [3]. From a theoretical point of view, the restriction to a fixed initial wave function has profound consequences. In particular, in contrast to the stationary case, physical observables are not just functionals of the density but also depend on the initial state. All examples discussed in this chapter, however, refer to systems that are in stationary equilibrium at the outset. The Hohenberg-Kohn theorem can be applied in this case and ensures that the ground-state wave function before the onset of the time-dependent perturbation is uniquely determined by the static density (up to an irrelevant phase factor). There is hence no explicit initial-state dependence in this scenario, and all observables are indeed pure functionals of the density alone.

2.2 The Time-Dependent Kohn-Sham Equations

Although the Runge-Gross theorem asserts that all observables are uniquely determined by the density, it makes no statement how this central quantity can actually be calculated. To overcome the analogous problem in static density-functional theory, Kohn and Sham [4] suggested to use an auxiliary system of noninteracting electrons moving in an effective local potential, which is designed in such a way that the densities of the auxiliary Kohn-Sham system and the real interacting electrons coincide. This idea can be generalised to the time-dependent case, where the Kohn-Sham electrons obey [2]

$$i\hbar \frac{\partial}{\partial t} \varphi_k(\mathbf{r}, t) = \left(-\frac{\hbar^2}{2m} \nabla^2 + V_{\text{eff}}(\mathbf{r}, t) \right) \varphi_k(\mathbf{r}, t) \quad (10)$$

and the density is given by

$$n(\mathbf{r}, t) = \sum_{k=1}^{\infty} f_k |\varphi_k(\mathbf{r}, t)|^2, \quad (11)$$

where f_k denotes the occupation numbers in the ground state. The important question whether one can always find a local potential $V_{\text{eff}}(\mathbf{r}, t)$ with the property that the orbitals obtained from the Kohn-Sham equations (10) reproduce the given density of an interacting electron system has been answered affirmative: if such a potential exists for the original stationary state, i.e., if the initial static ground-state density is “noninteracting V -representable”, then this remains true after the onset of an arbitrary time-dependent perturbation [5]. Furthermore, since the Runge-Gross theorem applies equally to noninteracting systems, the effective potential is then determined uniquely up to an irrelevant purely time-dependent function.

We have thus established the existence of an effective potential, but we must still find an explicit expression for use in practical calculations. As in static density-functional theory, we start with the separation

$$V_{\text{eff}}(\mathbf{r}, t) = V_{\text{ext}}(\mathbf{r}, t) + V_{\text{H}}(\mathbf{r}, t) + V_{\text{xc}}(\mathbf{r}, t), \quad (12)$$

where the first term is the external potential, the second is the Hartree potential

$$V_{\text{H}}(\mathbf{r}, t) = \int \frac{e^2}{|\mathbf{r} - \mathbf{r}'|} n(\mathbf{r}', t) d^3r' \quad (13)$$

accounting for the electrostatic interaction between the electrons and the third term incorporates all remaining exchange and correlation effects. In the stationary case one exploits the variational principle for the total-energy functional and determines the orbitals of the Kohn-Sham electrons in such a way that the energy is minimised. All potential terms are then well defined as functional derivatives of the corresponding energy contributions with respect to the density. In systems driven by time-dependent external fields the total energy is not a conserved quantity, however, and there is hence no minimisation principle for it. As an alternative one can use the quantum-mechanical action

$$A[\Phi] = \int_{t_0}^{t_1} dt \int \Phi^*(\mathbf{r}_1, \dots, \mathbf{r}_N; t) \left(i\hbar \frac{\partial}{\partial t} - H(t) \right) \Phi(\mathbf{r}_1, \dots, \mathbf{r}_N; t) d^3r_1 \dots d^3r_N. \quad (14)$$

The action has the property that its functional derivative with respect to $\Phi^*(\mathbf{r}_1, \dots, \mathbf{r}_N; t)$ vanishes at the true many-body wave function, i.e., the solution of the Schrödinger equation

$$\left. \frac{\delta A[\Phi]}{\delta \Phi^*(\mathbf{r}_1, \dots, \mathbf{r}_N; t)} \right|_{\Phi(\mathbf{r}_1, \dots, \mathbf{r}_N; t) = \Psi(\mathbf{r}_1, \dots, \mathbf{r}_N; t)} = \left(i\hbar \frac{\partial}{\partial t} - H(t) \right) \Psi(\mathbf{r}_1, \dots, \mathbf{r}_N; t) = 0. \quad (15)$$

Therefore, it is possible to solve the time-dependent problem by searching for the stationary point of the action. In contrast to the energy in the static case, there is no minimisation principle, however, as the stationary point is not necessarily a minimum. Furthermore, the value of the action itself does not provide any relevant additional information, since $A[\Psi] = 0$.

By virtue of the Runge-Gross theorem, we may consider the action as a functional of the density. The obvious definition of $A[n]$ is to evaluate Eq. (14) at the wave function $\Phi([n]; \mathbf{r}_1, \dots, \mathbf{r}_N; t)$ associated with $n(\mathbf{r}, t)$. In analogy to the total energy in static density-functional theory, the action may be decomposed as

$$A[n] = T_{\text{KS}}[n] - \int_{t_0}^{t_1} dt \int V_{\text{ext}}(\mathbf{r}, t) n(\mathbf{r}, t) d^3r - A_{\text{H}}[n] - A_{\text{xc}}[n] , \quad (16)$$

where $T_{\text{KS}}[n]$ denotes the kinetic contribution of the Kohn-Sham system

$$T_{\text{KS}}[n] = \sum_{k=1}^{\infty} f_k \int_{t_0}^{t_1} dt \int \varphi_k^*(\mathbf{r}, t) \left(i\hbar \frac{\partial}{\partial t} + \frac{\hbar^2}{2m} \nabla^2 \right) \varphi_k(\mathbf{r}, t) d^3r . \quad (17)$$

The third term on the right-hand side is linked to the Hartree potential and given explicitly by

$$A_{\text{H}}[n] = \frac{1}{2} \int_{t_0}^{t_1} dt \int n(\mathbf{r}, t) \frac{e^2}{|\mathbf{r} - \mathbf{r}'|} n(\mathbf{r}', t) d^3r d^3r' . \quad (18)$$

Its functional derivative with respect to the density yields $V_{\text{H}}(\mathbf{r}, t) = \delta A_{\text{H}}[n] / \delta n(\mathbf{r}, t)$. The final term $A_{\text{xc}}[n]$ incorporates all remaining exchange and correlation contributions. One would expect that the time-dependent exchange-correlation potential is likewise obtained as

$$V_{\text{xc}}(\mathbf{r}, t) = \frac{\delta A_{\text{xc}}[n]}{\delta n(\mathbf{r}, t)} . \quad (19)$$

Unfortunately, it is not so straightforward. The problem becomes evident if we examine the second functional derivative

$$\frac{\delta V_{\text{xc}}(\mathbf{r}, t)}{\delta n(\mathbf{r}', t')} = \frac{\delta^2 A_{\text{xc}}[n]}{\delta n(\mathbf{r}, t) \delta n(\mathbf{r}', t')} . \quad (20)$$

Whereas the expression on the right-hand side is symmetric in (\mathbf{r}, t) and (\mathbf{r}', t') , the exchange-correlation potential can only be influenced by the density at earlier times. Therefore, causality dictates that the left-hand side must vanish for $t < t'$ but not for $t > t'$. The symmetry and causality requirements contradict each other and cannot be satisfied simultaneously. We are hence forced to conclude that the action is not a differentiable functional of the density. This problem can be resolved within the Keldysh formalism for nonequilibrium dynamics, in which the physical time $t(\tau)$ is parametrised by an underlying parameter τ called pseudotime [6]. Defining the action on the pseudotime contour instead of the real time axis guarantees the proper symmetry of the second functional derivative in (\mathbf{r}, τ) and (\mathbf{r}', τ') , while the exchange-correlation potential is obtained in analogy to Eq. (19) by restoring the physical time argument *after* performing the functional derivative with respect to $n(\mathbf{r}, \tau)$. It is not surprising that due to its mathematical complexity, this formal approach has resonated rather little with actual practitioners of TDDFT. In fact, the design of specific approximations for the exchange-correlation potential in time-dependent situations is still at a very early stage. Most calculations take a pragmatic point of view and simply use one of the established functionals of static density-functional

theory. The most popular choice is the adiabatic local-density approximation (ALDA), which replaces the exchange-correlation potential at the coordinates \mathbf{r} and t by that of the homogeneous electron gas with the same local density $n(\mathbf{r}, t)$. It is readily expressed in terms of the exchange-correlation energy density $\epsilon_{xc}^{\text{hom}}(n)$ of the homogeneous electron gas according to

$$V_{xc}^{\text{ALDA}}(\mathbf{r}, t) = \frac{d}{dn} [n\epsilon_{xc}^{\text{hom}}(n)]_{n=n(\mathbf{r}, t)} . \quad (21)$$

The latter is known from quantum Monte-Carlo calculations [7] and available in parametrised form [8]. The ALDA is a rather drastic approximation that ignores the nonlocal dependence of $V_{xc}(\mathbf{r}, t)$ on the density elsewhere in space as well as the memory of the density distribution at earlier times. In addition, it inherits all the well known deficiencies of the stationary LDA, such as the incorrect exponential decay in front of surfaces, which suppresses the existence of bound image states. Nevertheless, there are few alternatives for practical calculations.

2.3 Excited States

Although TDDFT was originally developed to describe dynamic phenomena in time-dependent potentials, one of its principal areas of application today is the analysis of electronic excitations. This may at first seem surprising, because in popular perception density-functional theory is strongly associated with ground-state properties only. The information about the excited states is contained in the linear density-response function

$$\chi(\mathbf{r}, \mathbf{r}'; t - t') = \left. \frac{\delta n(\mathbf{r}, t)}{\delta V_{\text{ext}}(\mathbf{r}', t')} \right|_{V_{\text{ext}}(\mathbf{r}', t') = V_{\text{ext}}^{(0)}(\mathbf{r}')} . \quad (22)$$

Before discussing how this quantity can be accessed within TDDFT, here we first examine its connection with the electronic excitation spectrum. We consider the following situation: The system is initially at rest in a static potential $V_{\text{ext}}^{(0)}(\mathbf{r})$. The corresponding ground-state density is labeled $n^{(0)}(\mathbf{r})$. At the time t_0 an additional time-dependent perturbation $V_{\text{ext}}^{(1)}(\mathbf{r}, t)$ is switched on, so that the total external potential becomes $V_{\text{ext}}(\mathbf{r}, t) = V_{\text{ext}}^{(0)}(\mathbf{r}) + V_{\text{ext}}^{(1)}(\mathbf{r}, t)$. If the potential is sufficiently well behaved, then the induced change in the electron distribution can be expanded by orders of $V_{\text{ext}}^{(1)}(\mathbf{r}, t)$ according to $n(\mathbf{r}, t) = n^{(0)}(\mathbf{r}) + n^{(1)}(\mathbf{r}, t) + \dots$, where the first-order correction is just given by

$$n^{(1)}(\mathbf{r}, t) = \int_{-\infty}^{\infty} dt' \int d^3r' \chi(\mathbf{r}, \mathbf{r}'; t - t') V_{\text{ext}}^{(1)}(\mathbf{r}', t') \quad (23)$$

in terms of the linear density-response function. Causality requires $\chi(\mathbf{r}, \mathbf{r}'; t - t') = 0$ for $t < t'$, of course, because the density cannot be influenced by later variations of the potential.

The eigenstates of the original unperturbed Hamiltonian with the potential $V_{\text{ext}}^{(0)}(\mathbf{r})$ are labeled by $\Psi_j(\mathbf{r}_1, \dots, \mathbf{r}_N; t) = \Psi_j(\mathbf{r}_1, \dots, \mathbf{r}_N) \exp(-iE_j t/\hbar)$, where E_j denotes the corresponding energy eigenvalues. After the onset of the time-dependent perturbation, we expand the wave function $\Psi(\mathbf{r}_1, \dots, \mathbf{r}_N; t)$ that evolves from the ground state $\Psi^{(0)}(\mathbf{r}_1, \dots, \mathbf{r}_N; t) = \Psi_0(\mathbf{r}_1, \dots, \mathbf{r}_N; t)$ by orders of $V_{\text{ext}}^{(1)}(\mathbf{r}, t)$. The first-order correction is

$$\begin{aligned} \Psi^{(1)}(\mathbf{r}_1, \dots, \mathbf{r}_N; t) = & -\frac{i}{\hbar} \sum_{j=0}^{\infty} \Psi_j(\mathbf{r}_1, \dots, \mathbf{r}_N; t) \\ & \times \int_{-\infty}^{\infty} dt' \int \Psi_j^*(\mathbf{r}'_1, \dots, \mathbf{r}'_N; t') \sum_{k=1}^N V_{\text{ext}}^{(1)}(\mathbf{r}'_k, t') \Psi_0(\mathbf{r}'_1, \dots, \mathbf{r}'_N; t') \Theta(t - t') d^3r'_1 \dots d^3r'_N , \end{aligned} \quad (24)$$

as can easily be verified by inserting the series into the Schrödinger equation (1) and comparing the linear terms on both sides of the equal sign. The Heaviside step function $\Theta(t - t')$, which equals one for $t > t'$ and zero for $t < t'$, ensures the causality requirement. The corresponding change in the density is

$$\begin{aligned} n^{(1)}(\mathbf{r}, t) = & N \int \Psi^{(1)*}(\mathbf{r}, \mathbf{r}_2, \dots, \mathbf{r}_N; t) \Psi^{(0)}(\mathbf{r}, \mathbf{r}_2, \dots, \mathbf{r}_N; t) d^3r_2 \dots d^3r_N \\ & + N \int \Psi^{(0)*}(\mathbf{r}, \mathbf{r}_2, \dots, \mathbf{r}_N; t) \Psi^{(1)}(\mathbf{r}, \mathbf{r}_2, \dots, \mathbf{r}_N; t) d^3r_2 \dots d^3r_N. \end{aligned} \quad (25)$$

In order to simplify the notation, we introduce the overlap functions

$$n_j(\mathbf{r}) = N \int \Psi_0^*(\mathbf{r}, \mathbf{r}_2, \dots, \mathbf{r}_N) \Psi_j(\mathbf{r}, \mathbf{r}_2, \dots, \mathbf{r}_N) d^3r_2 \dots d^3r_N. \quad (26)$$

After inserting everything into Eq. (25) we obtain

$$\begin{aligned} n^{(1)}(\mathbf{r}, t) = & \int_{-\infty}^{\infty} dt' \int d^3r' \left[-\frac{i}{\hbar} \sum_{j=0}^{\infty} \left(n_j(\mathbf{r}) n_j^*(\mathbf{r}') e^{-i(E_j - E_0)(t - t')/\hbar} \right. \right. \\ & \left. \left. - n_j^*(\mathbf{r}) n_j(\mathbf{r}') e^{i(E_j - E_0)(t - t')/\hbar} \right) \Theta(t - t') \right] V_{\text{ext}}^{(1)}(\mathbf{r}', t'). \end{aligned} \quad (27)$$

If we compare this expression with Eq. (23), we eventually find that the term in square brackets equals the linear density-response function in the time domain. A straightforward Fourier transformation to frequency space is not possible, because the oscillating phase factors do not decay asymptotically, and consequently the integral over the positive time axis is indeterminate. We solve this problem by introducing an exponential damping term $\exp(-\eta(t - t')/\hbar)$ and taking the limit $\eta \rightarrow 0+$ after carrying out the integration. In this way we arrive at the final formula

$$\chi(\mathbf{r}, \mathbf{r}'; \omega) = \lim_{\eta \rightarrow 0+} \sum_{j=1}^{\infty} \left(\frac{n_j(\mathbf{r}) n_j^*(\mathbf{r}')}{\hbar\omega - (E_j - E_0) + i\eta} - \frac{n_j^*(\mathbf{r}) n_j(\mathbf{r}')}{\hbar\omega + (E_j - E_0) + i\eta} \right). \quad (28)$$

The ground state $j = 0$ does not contribute to the sum and has been omitted here. Note that the two terms in the brackets cancel because $n_0(\mathbf{r}) = n^{(0)}(\mathbf{r})$ is real-valued in this case. The important observation is that the poles of $\chi(\mathbf{r}, \mathbf{r}'; \omega)$ correspond to the exact excitation energies $E_j - E_0$. Furthermore, all quantities on the right-hand side depend only on the Hamiltonian of the unperturbed stationary system. By virtue of the Hohenberg-Kohn theorem, the linear density-response function is hence a functional of the static ground-state density $n^{(0)}(\mathbf{r})$.

2.4 Linear-Response Theory

To calculate the linear density-response function in practice, we exploit the fact that the density of the real system is identical to that of the noninteracting Kohn-Sham electrons. As the latter move in the effective potential $V_{\text{eff}}(\mathbf{r}'', t'')$, we apply the chain rule for functional derivatives

$$\chi(\mathbf{r}, \mathbf{r}'; t - t') = \int_{-\infty}^{\infty} dt'' \int d^3r'' \frac{\delta n(\mathbf{r}, t)}{\delta V_{\text{eff}}(\mathbf{r}'', t'')} \frac{\delta V_{\text{eff}}(\mathbf{r}'', t'')}{\delta V_{\text{ext}}(\mathbf{r}', t')}. \quad (29)$$

The first term on the right-hand side is the linear density-response function $\chi_{\text{KS}}(\mathbf{r}, \mathbf{r}''; t - t'')$ of the noninteracting Kohn-Sham system, defined in analogy to Eq. (22) but describing the change

in the density to first order in the total effective potential rather than the external potential. It can be derived following the same procedure as in the previous section and is given by

$$\chi_{\text{KS}}(\mathbf{r}, \mathbf{r}''; \omega) = \lim_{\eta \rightarrow 0^+} \sum_{k=1}^{\infty} \sum_{l=1}^{\infty} (f_k - f_l) \frac{\varphi_k^*(\mathbf{r}) \varphi_l(\mathbf{r}) \varphi_k(\mathbf{r}'') \varphi_l^*(\mathbf{r}'')}{\hbar\omega - (\epsilon_l - \epsilon_k) + i\eta} \quad (30)$$

in frequency space. The energies ϵ_k in the denominator are the Kohn-Sham eigenvalues of the unperturbed stationary wave functions $\varphi_k(\mathbf{r})$. To evaluate the second term in Eq. (29) we use the separation (12), which yields

$$\frac{\delta V_{\text{eff}}(\mathbf{r}'', t'')}{\delta V_{\text{ext}}(\mathbf{r}', t')} = \delta(\mathbf{r}'' - \mathbf{r}') \delta(t'' - t') + \frac{\delta V_{\text{H}}(\mathbf{r}'', t'')}{\delta V_{\text{ext}}(\mathbf{r}', t')} + \frac{\delta V_{\text{xc}}(\mathbf{r}'', t'')}{\delta V_{\text{ext}}(\mathbf{r}', t')} . \quad (31)$$

As both the Hartree potential and the exchange-correlation potential are given as functionals of the density, we apply the chain rule once more and rewrite these two contributions as

$$\frac{\delta V_{\text{H}}(\mathbf{r}'', t'')}{\delta V_{\text{ext}}(\mathbf{r}', t')} + \frac{\delta V_{\text{xc}}(\mathbf{r}'', t'')}{\delta V_{\text{ext}}(\mathbf{r}', t')} = \int_{-\infty}^{\infty} dt''' \int d^3r''' \left(\frac{\delta V_{\text{H}}(\mathbf{r}'', t'')}{\delta n(\mathbf{r}''', t''')} + \frac{\delta V_{\text{xc}}(\mathbf{r}'', t'')}{\delta n(\mathbf{r}''', t''')} \right) \frac{\delta n(\mathbf{r}''', t''')}{\delta V_{\text{ext}}(\mathbf{r}', t')} . \quad (32)$$

The last term on the right-hand side is easily recognised as the linear density-response function $\chi(\mathbf{r}''', \mathbf{r}'; t''' - t')$. The functional derivative of the Hartree potential with respect to the density follows directly from the definition (13) and simply equals the Coulomb potential

$$\frac{\delta V_{\text{H}}(\mathbf{r}'', t'')}{\delta n(\mathbf{r}''', t''')} = \frac{e^2}{|\mathbf{r}'' - \mathbf{r}'''|} \delta(t'' - t''') . \quad (33)$$

The final ingredient is the so-called exchange-correlation kernel

$$f_{\text{xc}}(\mathbf{r}'', \mathbf{r}'''; t'' - t''') = \left. \frac{\delta V_{\text{xc}}(\mathbf{r}'', t'')}{\delta n(\mathbf{r}''', t''')} \right|_{n(\mathbf{r}'', t'')=n^{(0)}(\mathbf{r}'')} . \quad (34)$$

After collecting all terms and Fourier transforming to frequency space, whereby convolutions on the time axis turn into simple multiplications, we obtain the final integral equation [9]

$$\begin{aligned} \chi(\mathbf{r}, \mathbf{r}'; \omega) &= \chi_{\text{KS}}(\mathbf{r}, \mathbf{r}'; \omega) \\ &+ \int d^3r'' \int d^3r''' \chi_{\text{KS}}(\mathbf{r}, \mathbf{r}''; \omega) \left(\frac{e^2}{|\mathbf{r}'' - \mathbf{r}'''|} + f_{\text{xc}}(\mathbf{r}'', \mathbf{r}'''; \omega) \right) \chi(\mathbf{r}''', \mathbf{r}'; \omega) . \end{aligned} \quad (35)$$

Practical implementations of TDDFT solve this integral equation routinely by projecting all quantities onto a suitable set of orthonormal basis functions, thus turning it into a matrix equation $\chi(\omega) = \chi_{\text{KS}}(\omega) + \chi_{\text{KS}}(\omega)[v + f_{\text{xc}}(\omega)]\chi(\omega)$ that is more suitable for a numerical treatment. The linear density-response function in this representation is then obtained by matrix inversion and given in closed form by $\chi(\omega) = \{1 - \chi_{\text{KS}}(\omega)[v + f_{\text{xc}}(\omega)]\}^{-1} \chi_{\text{KS}}(\omega)$.

2.5 The Exchange-Correlation Kernel

The central ingredient for the calculation of the linear density-response function according to Eq. (35) is the exchange-correlation kernel $f_{\text{xc}}(\mathbf{r}, \mathbf{r}'; \omega)$, formally defined as the functional

derivative of the exchange-correlation potential with respect to the density. Any explicit formula for the potential can hence, in principle, be used to derive a matching approximation for the kernel. The most common expression, the adiabatic local-density approximation [10]

$$f_{xc}^{\text{ALDA}}(\mathbf{r}, \mathbf{r}'; t - t') = \frac{\delta V_{xc}^{\text{ALDA}}(\mathbf{r}, t)}{\delta n(\mathbf{r}', t')} = \delta(\mathbf{r} - \mathbf{r}') \delta(t - t') \frac{d^2}{dn^2} [n \epsilon_{xc}^{\text{hom}}(n)]_{n=n^{(0)}(\mathbf{r})}, \quad (36)$$

is indeed obtained in this way. Although it is based on a numerically exact parametrisation of the exchange-correlation energy density $\epsilon_{xc}^{\text{hom}}(n)$ for the homogeneous electron gas with constant density n , it is important to realise that the ALDA actually constitutes a very poor representation of the kernel even for homogeneous systems. In contrast to the true exchange-correlation kernel $f_{xc}^{\text{hom}}(|\mathbf{r} - \mathbf{r}'|, t - t')$ of the homogeneous electron gas, it is local both in the space and time coordinates, thus ignoring essential physical features like the nonlocal dependence on the global density distribution or the memory of the density at former times. In fact, in reciprocal space the ALDA corresponds only to the long-wavelength limit $f_{xc}^{\text{ALDA}}(q, \omega) = \lim_{q \rightarrow 0} f_{xc}^{\text{hom}}(q, 0)$ at $\omega = 0$. The static exchange-correlation potential in bulk solids, on the other hand, is typically modeled quite well by the LDA; in the case of the homogeneous electron gas it yields the correct constant potential. To ensure an accurate overall description, the potential and kernel are hence often treated independently, and separate approximations are made for both quantities.

Unfortunately, very little is known about the properties of the true exchange-correlation kernel. First of all, causality requires $f_{xc}(\mathbf{r}, \mathbf{r}'; t - t') = 0$ for $t < t'$. A few straightforward symmetry relations can be inferred from the inversion of the integral equation (35). As the density is a real-valued quantity, the linear density-response function and hence the kernel must also be real in the time domain, which implies $f_{xc}(\mathbf{r}, \mathbf{r}'; \omega) = f_{xc}^*(\mathbf{r}, \mathbf{r}'; -\omega)$ after Fourier transformation to the frequency axis. Besides, the linear density-response function is symmetric in its two spatial arguments if the unperturbed stationary system exhibits time-reversal symmetry, so that $f_{xc}(\mathbf{r}, \mathbf{r}'; \omega) = f_{xc}(\mathbf{r}', \mathbf{r}; \omega)$ in the absence of magnetic fields. Some additional constraints can be obtained from general considerations. For example, the generic high-frequency behaviour $f_{xc}(\mathbf{r}, \mathbf{r}'; \omega) = f_{xc}(\mathbf{r}, \mathbf{r}'; \infty) + O(1/\omega^2)$ follows from the known asymptotic properties of $\chi(\mathbf{r}, \mathbf{r}'; \omega)$ and $\chi_{\text{KS}}(\mathbf{r}, \mathbf{r}'; \omega)$. In general, however, further progress can only be made if a specific system is considered. For the homogeneous electron gas, in particular, a large number of exact sum rules and asymptotic limits have been derived. In combination with an explicit evaluation of the leading correlation terms, which reveal the basic shape of $f_{xc}^{\text{hom}}(q, \omega)$, these can be exploited to construct a highly accurate expression for the dynamic exchange-correlation kernel [11]. The static kernel at $\omega = 0$ can alternatively be calculated by quantum Monte-Carlo techniques [12].

Although parametrisations of $f_{xc}^{\text{hom}}(|\mathbf{r} - \mathbf{r}'|, t - t')$ for a wide range of densities are readily available, it is difficult to employ these in calculations for real materials, because it is unclear how to choose the density parameter uniquely in inhomogeneous systems where, in general, $n^{(0)}(\mathbf{r}) \neq n^{(0)}(\mathbf{r}')$. Nevertheless, for the homogeneous electron gas this makes it possible to determine the excitation spectrum with high precision and to identify the important features that simpler approximations for the kernel must retain. As an illustration, Fig. 1 shows the excitation energies of the homogeneous electron gas obtained from the poles of the linear density-response function $\chi(q, \omega) = \chi_{\text{KS}}(q, \omega) / \{1 - \chi_{\text{KS}}(q, \omega)[v(q) + f_{xc}(q, \omega)]\}$ with $v(q) = 4\pi e^2/q^2$ and different approximations for the exchange-correlation kernel [13]. The density $n = 0.0252 \text{ \AA}^{-3}$ equals that of sodium. The grey-shaded region indicates the continuum of electron-hole pair excitations, which correspond to the singularities $\hbar\omega = \epsilon_{k'} - \epsilon_k$ of the numerator $\chi_{\text{KS}}(q, \omega)$, where ϵ_k and $\epsilon_{k'}$ denotes the eigenvalue of an occupied and an unoccupied Kohn-Sham state,

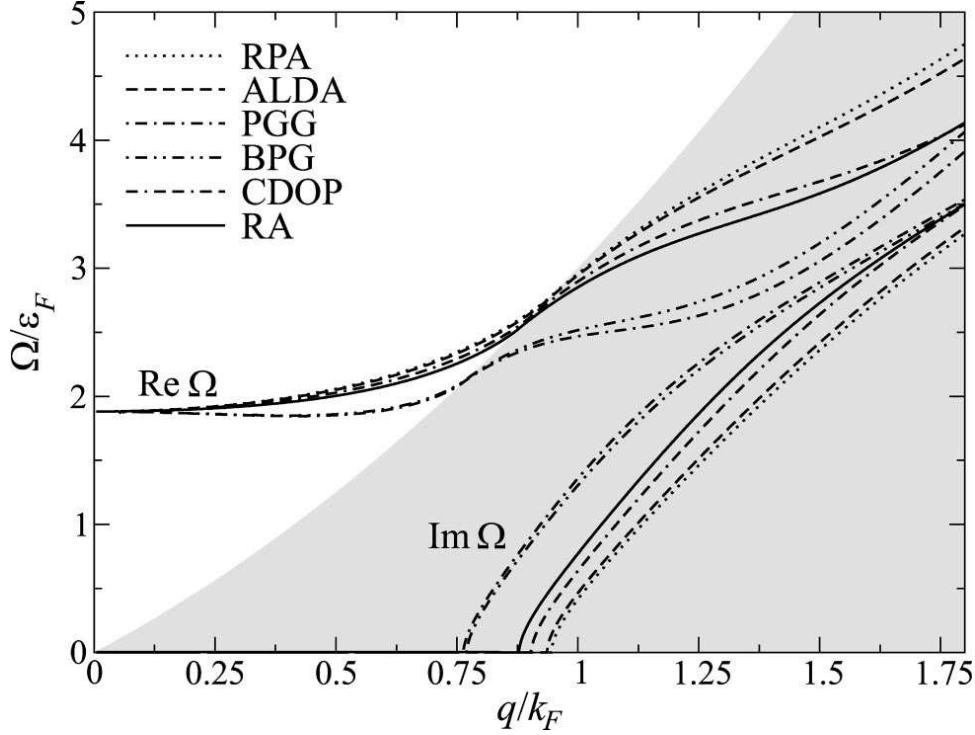


Fig. 1: Plasmon dispersion Ω_q for the homogeneous electron gas, calculated with six different approximations for the exchange-correlation kernel. The real and imaginary parts are shown separately. The grey-shaded region indicates the electron-hole pair continuum, where the plasmons are strongly damped. Taken from Ref. [13].

respectively, and $\mathbf{q} = \mathbf{k}' - \mathbf{k}$. In addition, there is a distinct plasmon branch Ω_q , which describes collective charge oscillations of the electron system and corresponds to the zeroes of the denominator, i.e., the solutions of

$$1 - \chi_{\text{KS}}(q, \Omega_q/\hbar) [v(q) + f_{\text{xc}}(q, \Omega_q/\hbar)] = 0. \quad (37)$$

We focus on the latter, because the results directly reflect the quality of the kernel. The axes in the figure are scaled in units of the Fermi wave vector $k_F = \sqrt[3]{3\pi^2 n} = 0.907 \text{ \AA}^{-1}$ and the Fermi energy $\epsilon_F = \hbar^2 k_F^2 / 2m = 3.13 \text{ eV}$. The plasmon branch starts at the classical plasma frequency $\Omega_0 = \sqrt{4\pi n e^2 / m} = 5.89 \text{ eV}$. For small wave vectors energy and momentum conservation do not allow a decay into electron-hole pairs. The plasmons hence have a long lifetime, but inside the electron-hole pair continuum they are strongly damped. In this region the solutions of Eq. (37) become complex numbers $\Omega_q = \Omega'_q - i\Omega''_q$ with $\Omega''_q > 0$. Mathematically, the sum over a few effective spectral features with complex energies in Eq. (28) is equivalent to the integration over a continuum of excited states with real energies and infinitesimal imaginary parts. In the time domain the imaginary part Ω''_q gives rise to an additional exponential damping term $\exp(-\Omega''_q(t - t')/\hbar)$, which can be interpreted as a finite lifetime \hbar/Ω''_q . The imaginary part Ω''_q of the plasmon energies is shown separately in the figure.

As the parametrisation of the dynamic exchange-correlation kernel by Richardson and Ashcroft (RA) [11] is believed to be very close to the exact function, it can be taken as a reference to assess the performance of more simplified schemes. The comparison with different common approximations allows us to draw the following conclusions.

1. The parametrisation of the static exchange-correlation kernel by Corradini, Del Sole,

Onida and Palumbo (CDOP) [14], based on numerically exact Monte-Carlo data [12], retains the full spatial nonlocality but neglects the frequency dependence. The dispersion differs little from the results obtained with the dynamic RA kernel. This suggests that the frequency dependence is, in fact, not crucial for the calculation of excited states.

2. The ALDA further ignores the spatial nonlocality. The dispersion agrees well with the reference results in the limit of small wave vectors, where the ALDA exhibits the correct asymptotic behaviour, but shows an increasing discrepancy at larger wave vectors, which indicates that the spatial nonlocality of the kernel is an important feature.
3. This point is further stressed by the poor performance of the parametrisations by Petersilka, Gossmann and Gross (PGG) [9] and by Burke, Petersilka and Gross (BPG) [15]. Both kernels were specifically designed for few-electron systems in molecular physics and do not incorporate the correct asymptotic behaviour of the homogeneous electron gas. Consequently, the calculated curves show a strong deviation from the true plasmon dispersion even for small wave vectors.
4. Finally, the random-phase approximation (RPA) neglects dynamic exchange-correlation effects altogether by setting $f_{xc}^{\text{RPA}}(\mathbf{r}, \mathbf{r}'; t - t') = 0$. Compared to this simplest possible treatment, the ALDA constitutes a small but definite improvement at all wave vectors.

Although based on data for the homogeneous electron gas, these conclusions remain generally valid for inhomogeneous systems. In applications of TDDFT to real materials the ALDA can often be expected to yield excitation spectra with sufficient accuracy for practical purposes; if significant deviations from experimental measurements are observed, then it is usually because of the oversimplified wave-vector dependence. One example where a more careful treatment of the spatial nonlocality is necessary to obtain reliable results is the study of optical absorption in semiconductors, which is discussed at the end of the following section.

3 Applications in Theoretical Spectroscopy

In this section we discuss the theoretical simulation of two spectroscopic techniques, electron energy-loss spectroscopy and optical absorption. In both cases the measured spectra can be related directly to the linear density-response function.

3.1 Electron Energy-Loss Spectroscopy

Electron energy-loss spectroscopy (EELS) is a well-established and very useful tool to study electronic excitations in solids. In the experiment a beam of electrons with initial wave vector \mathbf{k}_i and kinetic energy $\epsilon_i = \hbar^2 k_i^2 / 2m$ impinges on a sample and loses energy through inelastic scattering processes by exciting electron-hole pairs, plasmons or other collective modes. Depending on the setup, the impinging particles either travel through the material or scatter from it. In the first case they mainly probe the electronic structure of the bulk, in the second they are sensitive to surface characteristics. A detector positioned at angles θ and ϕ relative to the original beam direction measures the final kinetic energy $\epsilon_f = \hbar^2 k_f^2 / 2m$ of the electrons, which also yields the wave vector $\mathbf{k}_f = k_f(\sin \theta \cos \phi, \sin \theta \sin \phi, \cos \theta)$. The energy loss $\hbar\omega = \epsilon_i - \epsilon_f$ quantifies the energy transferred from the incident electron to the system. The differential cross section per solid angle $d\Omega = \sin \theta d\theta d\phi$ and energy $d(\hbar\omega)$ for the scattering of an electron

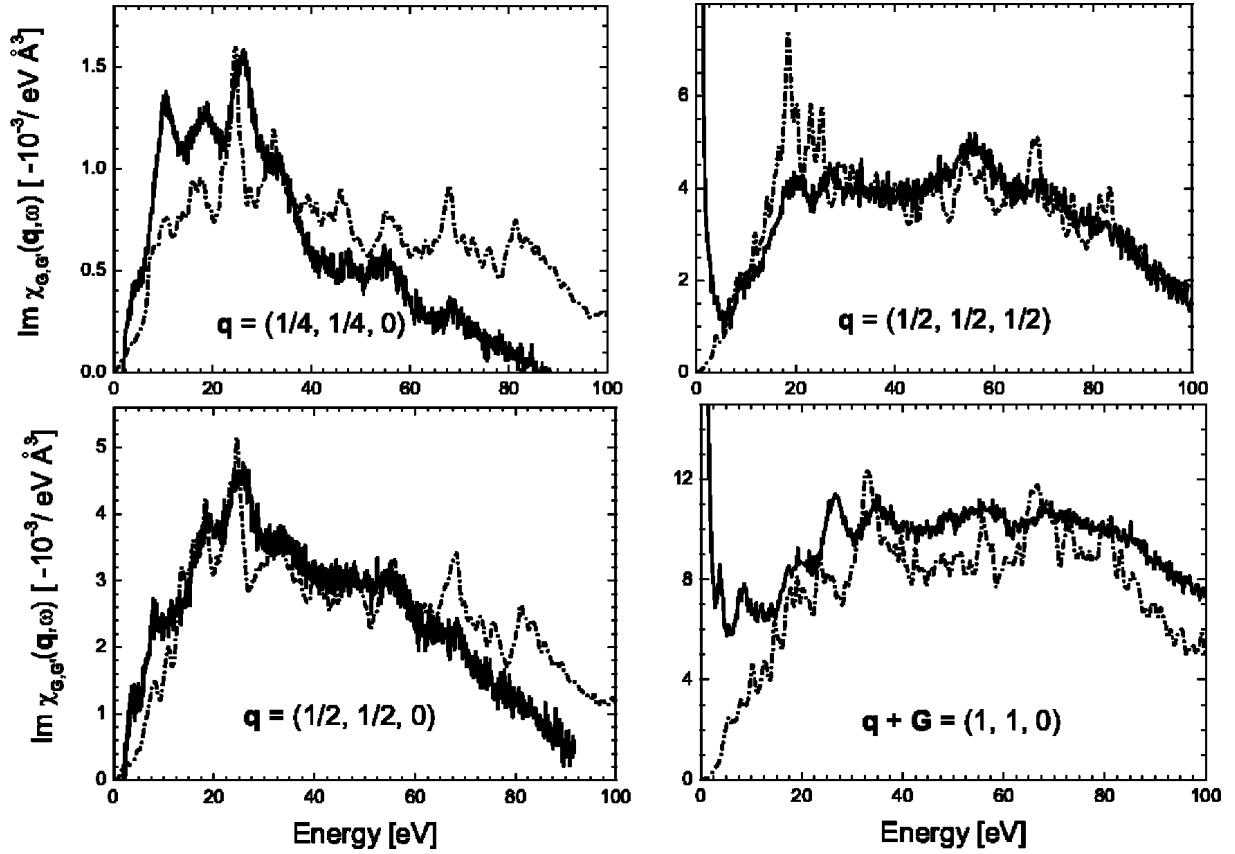


Fig. 2: Comparison of the diagonal elements $\text{Im } \chi_{GG'}(\mathbf{q}, \omega)$ with $\mathbf{G} = \mathbf{G}'$ calculated within the ALDA (dot-dashed lines) to experimental EELS spectra (solid lines) for silver. The wave vectors are given in units of $2\pi/a$ with the lattice constant $a = 4.09 \text{ \AA}$. Taken from Ref. [17].

beam from a many-body target can be calculated within first-order time-dependent perturbation theory, the so-called first Born approximation, and is given by [16]

$$\frac{d^2\sigma}{d\Omega d(\hbar\omega)} = \frac{m^2}{(2\pi)^2 \hbar^4} v(\mathbf{k}_i - \mathbf{k}_f)^2 \frac{k_f}{k_i} S(\mathbf{k}_i - \mathbf{k}_f, \omega), \quad (38)$$

where $v(\mathbf{k}_i - \mathbf{k}_f) = 4\pi e^2/|\mathbf{k}_i - \mathbf{k}_f|^2$ is again the Fourier transform of the Coulomb potential. Most factors on the right-hand side are controlled by the explicit experimental setup and do not depend on the sample. The only material-specific term is the dynamic structure factor

$$S(\mathbf{k}_i - \mathbf{k}_f, \omega) = -\frac{1}{\pi} \text{Im } \chi_{\mathbf{G}\mathbf{G}}(\mathbf{q}, \omega), \quad (39)$$

where the transferred wave vector $\mathbf{k}_i - \mathbf{k}_f = \mathbf{q} + \mathbf{G}$ is decomposed in such a way that \mathbf{q} lies inside the first Brillouin zone and \mathbf{G} is a reciprocal lattice vector. Therefore, EELS allows a direct experimental measurement of the diagonal elements of the linear density-response function

$$\chi_{\mathbf{G}\mathbf{G}'}(\mathbf{q}, \omega) = \int e^{-i(\mathbf{q}+\mathbf{G})\cdot\mathbf{r}} \chi(\mathbf{r}, \mathbf{r}'; \omega) e^{i(\mathbf{q}+\mathbf{G}')\cdot\mathbf{r}'} d^3r d^3r' \quad (40)$$

in reciprocal space and gives access to the information about excited states contained in it. The imaginary part of the linear density-response function for silver obtained within the ALDA [17] is shown in Fig. 2 and compared to experimental EELS spectra. The implementation

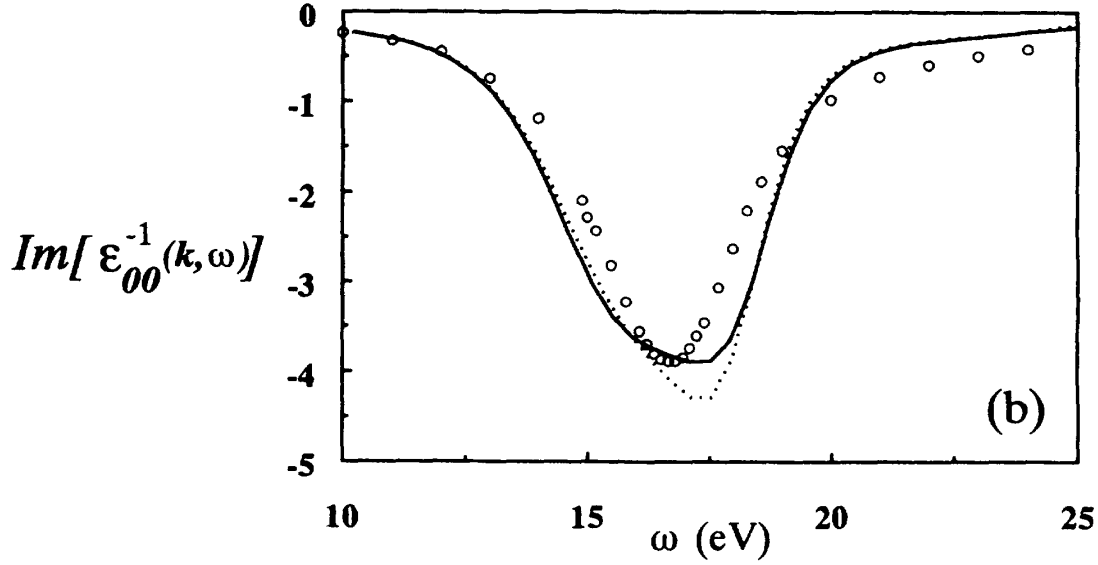


Fig. 3: Comparison of $\text{Im} \varepsilon_{00}^{-1}(\mathbf{q}, \omega)$ in the limit $\mathbf{q} \rightarrow 0$ calculated within the ALDA (dotted line) and RPA (solid line) to experimental EELS data (circles) for silicon. Taken from Ref. [18].

is based on the plane-wave pseudopotential method with an energy cutoff of 130 Ry for the expansion of the Kohn-Sham wave functions and 90 bands in the sums over eigenstates in Eq. (30), including 4s and 4p semi-core states. This incorporates transitions up to 150 eV above the Fermi energy. The data are shown as a function of the energy $\hbar\omega$ for four different wave vectors $\mathbf{q} + \mathbf{G}$ given in units of $2\pi/a$, where $a = 4.09 \text{ \AA}$ is the experimental lattice constant of silver. The theoretical results are in good overall agreement with the measured spectra and reproduce the characteristic profiles for the different wave vectors correctly. The remaining discrepancy, especially at high energy loss, may signal a failure of the ALDA but is more likely due to the occurrence of multiple-scattering events not captured by the first Born approximation (38).

As another example, Fig. 3 shows results for silicon in the limit $\mathbf{q} \rightarrow 0$ obtained in a similar way [18], this time expressed in terms of the inverse microscopic dielectric function

$$\varepsilon^{-1}(\mathbf{r}, \mathbf{r}'; t - t') = \delta(\mathbf{r} - \mathbf{r}')\delta(t - t') + \int v(\mathbf{r} - \mathbf{r}'')\chi(\mathbf{r}'', \mathbf{r}'; t - t') d^3r'', \quad (41)$$

which implies $\text{Im} \varepsilon_{\mathbf{G}\mathbf{G}}^{-1}(\mathbf{q}, \omega) = v(\mathbf{q} + \mathbf{G}) \text{Im} \chi_{\mathbf{G}\mathbf{G}}(\mathbf{q}, \omega)$ in reciprocal space. The broad peak near 16.5 eV is a plasmon resonance. Both the RPA and the ALDA curves are very close to the experimental data, which indicates that dynamic exchange-correlation effects only play a minor role in this case. The situation is thus akin to that of plasmons in the homogeneous electron gas (see Fig. 1), where the difference, in fact, vanishes exactly in the long-wavelength limit as both dispersion curves approach the classical plasma frequency.

3.2 Optical Absorption

Optical absorption is a different kind of spectroscopy in which solids are irradiated with light rather than particle beams. The absorption strength at a given frequency ω is in practice determined by measuring the transmission or reflection of the incident light. The quantity probed in this way is the imaginary part $\text{Im} \varepsilon_M(\omega)$ of the macroscopic dielectric function. In contrast to EELS, there is no \mathbf{q} -dependence in this case, because the momentum of the photons is negligible compared to that of the electrons. The macroscopic dielectric function is related to the head

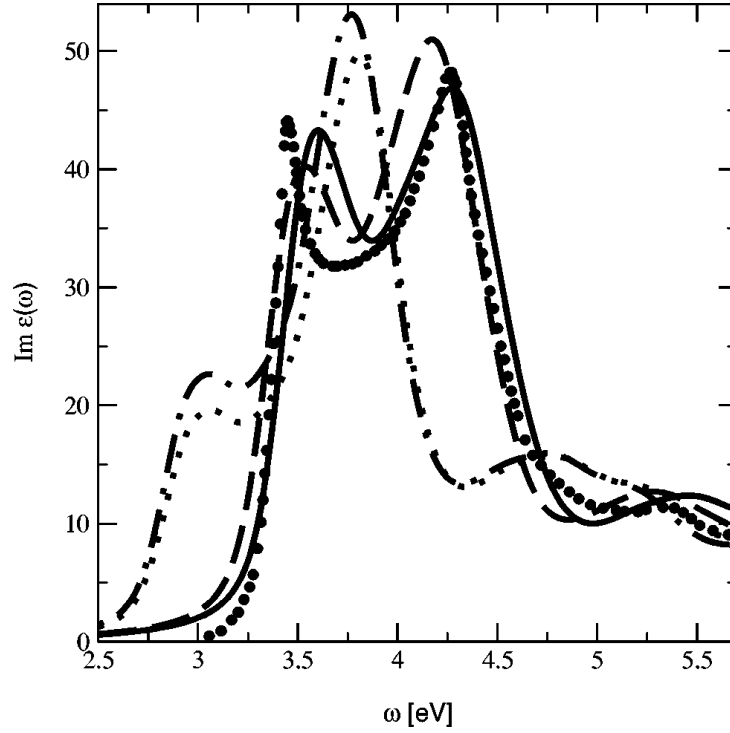


Fig. 4: Optical absorption spectrum $\text{Im } \epsilon_M(\omega)$ of silicon calculated within the RPA (dotted line), ALDA (dot-dashed line), TDDFT with a long-range kernel (solid line) and the Bethe-Salpeter equation of many-body perturbation theory (long-dashed line), compared to experimental data (circles). Taken from Ref. [19].

of the inverse microscopic dielectric matrix by

$$\epsilon_M(\omega) = \lim_{\mathbf{q} \rightarrow 0} \frac{1}{\epsilon_{00}^{-1}(\mathbf{q}, \omega)} . \quad (42)$$

If the microscopic dielectric matrix is diagonal in the reciprocal lattice vectors, then Eq. (42) reduces to $\epsilon_M(\omega) = \lim_{\mathbf{q} \rightarrow 0} \epsilon_{00}(\mathbf{q}, \omega)$, and the macroscopic dielectric function simply equals the spatial average of the microscopic function. This is the case in the homogeneous electron gas. For all other materials the matrix $\epsilon_{\mathbf{G}\mathbf{G}'}(\mathbf{q}, \omega)$ is nondiagonal, however, which means that not only the head but also all other matrix elements contribute to $\epsilon_M(\omega)$ through the inversion. Their combined influence is known as local-field effects and arises in inhomogeneous systems because external perturbations induce fluctuations on the atomic scale, which themselves generate additional internal microscopic fields that must be taken into account.

The optical absorption spectrum of silicon in Fig. 4 shows the typical characteristics of a semiconductor. In the infrared regime the material is transparent, because the energy of the photons is not sufficient to excite electrons across the fundamental band gap. At higher frequencies the experimental spectrum exhibits two pronounced peaks. The first is a sharp exciton resonance and describes the formation of bound electron-hole pairs. The second, broader feature corresponds to interband transitions from the valence into the conduction band. The theoretical results for $\epsilon_M(\omega)$ were obtained by evaluating Eq. (42) with the microscopic dielectric function (41) and using different exchange-correlation kernels for the linear density-response function [19]. The RPA and ALDA kernels again yield very similar results. Although the entire spectrum is shifted to lower energies, the second peak is clearly discernible and has approximately

the correct weight and line shape. This is not surprising, as the interband transitions are already included in $\chi_{\mathbf{G}\mathbf{G}'}^{\text{KS}}(\mathbf{q}, \omega)$. The displacement towards lower energies reflects the underestimation of the fundamental band gap within density-functional theory. The first peak, on the other hand, is poorly reproduced, because the formation of excitons arises from intricate correlation effects that are not adequately described by the ALDA kernel.

Why does the ALDA yield such a poor optical absorption spectrum while the electron energy-loss curve in Fig. 3 is almost perfect? After all, both quantities are derived from the same linear density-response function. In order to understand this apparent contradiction, it is important to realise that the macroscopic dielectric function (42) can be rewritten as [20]

$$\varepsilon_{\text{M}}(\omega) = 1 - \lim_{\mathbf{q} \rightarrow 0} v(\mathbf{q}) \bar{\chi}_{00}(\mathbf{q}, \omega) \quad (43)$$

in terms of a new response function $\bar{\chi}_{\mathbf{G}\mathbf{G}'}(\mathbf{q}, \omega)$. The latter satisfies an integral equation

$$\bar{\chi}_{\mathbf{G}\mathbf{G}'}(\mathbf{q}, \omega) = \chi_{\mathbf{G}\mathbf{G}'}^{\text{KS}}(\mathbf{q}, \omega) + \sum_{\mathbf{G}'', \mathbf{G}'''} \chi_{\mathbf{G}\mathbf{G}''}^{\text{KS}}(\mathbf{q}, \omega) [\bar{v}(\mathbf{q} + \mathbf{G}'') \delta_{\mathbf{G}''\mathbf{G}'''} + f_{\mathbf{G}''\mathbf{G}'''}^{\text{xc}}(\mathbf{q}, \omega)] \bar{\chi}_{\mathbf{G}''\mathbf{G}'}(\mathbf{q}, \omega) \quad (44)$$

analogous to (35) but with the modified interaction

$$\bar{v}(\mathbf{q} + \mathbf{G}) = \begin{cases} 0 & \text{if } \mathbf{G} = \mathbf{0} , \\ v(\mathbf{q} + \mathbf{G}) = \frac{4\pi e^2}{|\mathbf{q} + \mathbf{G}|^2} & \text{otherwise .} \end{cases} \quad (45)$$

In contrast to the normal Coulomb interaction, $\bar{v}(\mathbf{q} + \mathbf{G})$ does not diverge as $\mathbf{q} + \mathbf{G} \rightarrow \mathbf{0}$ but drops to zero, which in turn implies that $\bar{v}(\mathbf{r} - \mathbf{r}')$ is short-ranged in real space. It is precisely this different behaviour at small wave vectors that is responsible for the observed features. The EELS spectrum $-\text{Im } \varepsilon_{00}^{-1}(\mathbf{q}, \omega) = -v(\mathbf{q}) \text{Im } \chi_{00}(\mathbf{q}, \omega)$ is calculated from the full linear density-response function (35). For small \mathbf{q} the Coulomb potential diverges and dominates over the exchange-correlation kernel. The ALDA, in particular, tends to a finite value and thus has a negligible influence in this limit, yielding almost the same results as the RPA. On the other hand, the optical absorption spectrum $\text{Im } \varepsilon_{\text{M}}(\omega) = -\lim_{\mathbf{q} \rightarrow 0} v(\mathbf{q}) \text{Im } \bar{\chi}_{00}(\mathbf{q}, \omega)$ includes the modified response function (44) calculated without the singularity of the Coulomb potential. Therefore, the exchange-correlation kernel dominates the spectral features in this case, and the failure of the ALDA becomes apparent. The true kernel in semiconductors is actually divergent at small wave vectors. This reflects the fact that screening is incomplete in materials with a band gap. Instead, a polarisation charge forms on the surface and gives rise to an additional long-range electric field. The ALDA cannot capture this effect, because it is based on a metallic reference system, the homogeneous electron gas. As a remedy, Reining et al. [19] suggested to use a divergent expression of the form $-\alpha e^2/q^2$, which corresponds to a long-range function $-\alpha e^2/(4\pi|\mathbf{r} - \mathbf{r}'|)$ in real space, instead of the ALDA in such cases. The results in Fig. 4, calculated with an empirical parameter $\alpha = 0.2$, confirm that this long-range kernel indeed improves the description of optical absorption spectra significantly. A survey of several other semiconducting materials suggests that this empirical value is a typical magnitude for α [21].

An alternative method that also yields the correct spectral features is the Bethe-Salpeter equation of many-body perturbation theory, which involves the calculation of a two-particle Green function for the correlated motion of electron-hole pairs [22]. The curve obtained in this way is displayed in Fig. 4 for comparison with the TDDFT results. Many-body perturbation theory has the appeal that the physical contents of approximations can be controlled in a very transparent

way; in this example the electron-hole attraction is explicitly included in the two-particle Green function to enable the description of excitons. On the other hand, the computational cost is much higher than that of a standard TDDFT calculation.

4 Summary

Although most applications of TDDFT are still in the field of atomic and molecular systems, it has long since also become an established method in condensed-matter physics. Its principal use here is the investigation of excited states, which can be obtained directly from the linear density-response function. As two typical examples, we discussed the theoretical simulation of electron energy-loss spectroscopy (EELS) and optical absorption. The results put a spotlight both on the success and the deficiencies of current implementations.

As TDDFT constitutes an exact mathematical formalism, the linear density-response function should, in principle, contain information about the complete excitation spectrum, independent of the physical nature of the excited states. Quantitative or even qualitative inaccuracies can only be due to approximations that are, of course, always necessary in practical implementations. Besides numerical convergence parameters, approximations must be chosen for the static exchange-correlation potential and the exchange-correlation kernel. Based on studies of finite systems, it is frequently claimed that the former is the more crucial quantity [15]. The reason is that common approximations like the LDA or generalised gradient approximations (GGA) wrongly predict a rapid exponential fall of the potential instead of a slow algebraic decay at large distances, with a negative effect on the description of unoccupied orbitals that may extend far into the vacuum. At the Kohn-Sham level these schemes hence provide a poor starting point for the study of molecular transition energies, while the local ALDA kernel performs well for small systems. In periodic solids, on the other hand, the asymptotic behaviour of the potential is of no relevance, and the LDA often gives a good qualitative picture of the electronic structure. At the same time, as illustrated by the examples in this chapter, the nonlocality of the kernel may become an important issue in extended systems with long-range correlation effects.

As the development of specific exchange-correlation functionals for time-dependent is still at an early stage, the only nontrivial kernel that is widely used in practical calculations is the ALDA. Although it is a local approximation, the calculated EELS spectra are typically in good agreement with experimental measurements, because long-range effects are dominated by the Coulomb potential and the kernel merely provides minor corrections. The excitations probed by this technique, especially plasmons, are hence obtained accurately. On the other hand, long-range exchange-correlation effects are crucial for the simulation of optical absorption spectra, and the ALDA consequently yields poor results in this case. In particular, it is unable to describe excitons in semiconductors. This failure initiated a search for better functionals, and some preliminary progress has already been made. The long-range kernel proposed by Reining et al. [19] succeeds in reproducing the exciton resonance in the optical absorption spectrum but relies on an empirical parameter to achieve agreement with the experimental data. In the future, parameter-free approaches will likely be based on a systematic evaluation by orders of the Coulomb potential. The leading term of first order, the exact exchange kernel, already exhibits the correct long-range behaviour [23], but its evaluation is currently still too expensive for routine calculations. Another direction of active research is the extension of TDDFT to treat the interaction of matter with time-dependent magnetic fields, which opens the way to investigate spin waves (magnons) and other characteristic excitations in magnetic systems [24].

Acknowledgments

The author thanks Christoph Friedrich for a critical reading of the manuscript and many helpful suggestions for improvements.

References

- [1] P. Hohenberg and W. Kohn, Phys. Rev. **136**, B864 (1964)
- [2] E. Runge and E. K. U. Gross, Phys. Rev. Lett. **52**, 997 (1984)
- [3] N. T. Maitra and K. Burke, Phys. Rev. A **63**, 042501 (2001)
- [4] W. Kohn and L. J. Sham, Phys. Rev. **140**, A1133 (1965)
- [5] R. van Leeuwen, Phys. Rev. Lett. **82**, 3863 (1999)
- [6] R. van Leeuwen, Phys. Rev. Lett. **80**, 1280 (1998)
- [7] D. M. Ceperley and B. J. Alder, Phys. Rev. Lett. **45**, 566 (1980)
- [8] J. P. Perdew and Y. Wang, Phys. Rev. B **46**, 12947 (1992); **56**, 7018(E) (1997)
- [9] M. Petersilka, U. J. Gossmann and E. K. U. Gross, Phys. Rev. Lett. **76**, 1212 (1996)
- [10] A. Zangwill and P. Soven, Phys. Rev. Lett. **45**, 204 (1980)
- [11] C. F. Richardson and N. W. Ashcroft, Phys. Rev. B **50**, 8170 (1994)
- [12] S. Moroni, D. M. Ceperley and G. Senatore, Phys. Rev. Lett. **75**, 689 (1995)
- [13] K. Tatarczyk, A. Schindlmayr and M. Scheffler, Phys. Rev. B **63**, 235106 (2001)
- [14] M. Corradini, R. Del Sole, G. Onida and M. Palumbo, Phys. Rev. B **57**, 14569 (1998)
- [15] K. Burke, M. Petersilka and E. K. U. Gross, in *Recent Advances in Density Functional Methods*, edited by V. Barone, P. Fantucci and A. Bencini (World Scientific, Singapore, 2002), Vol. III, p. 67
- [16] P. Nozières, *Theory of Interacting Fermi Systems* (Addison-Wesley, Reading, 1997)
- [17] W.-D. Schöne, D. S. Su and W. Ekardt, Phys. Rev. B **68**, 115102 (2003)
- [18] R. Daling, W. van Haeringen and B. Farid, Phys. Rev. B **45**, 8970 (1992)
- [19] L. Reining, V. Olevano, A. Rubio and G. Onida, Phys. Rev. Lett. **88**, 066404 (2002)
- [20] W. Hanke, Adv. Phys. **27**, 287 (1978)
- [21] W. G. Aulbur, L. Jönsson and J. W. Wilkins, Phys. Rev. B **54**, 8540 (1996)
- [22] S. Albrecht, L. Reining, R. Del Sole and G. Onida, Phys. Rev. Lett. **80**, 4510 (1998)
- [23] Y.-H. Kim and A. Görling, Phys. Rev. Lett. **89**, 096402 (2002)
- [24] S. Y. Savrasov, Phys. Rev. Lett. **81**, 2570 (1998)